1

Solution Chemistry of Iron

1.1 Iron Chemistry

In the Earth's crust, iron is the fourth most abundant element and the second most abundant metal (the most abundant is aluminium). Situated in the Periodic Table in the middle of the first transition series (characterised by having incompletely filled d orbitals), iron has access to a number of oxidation states (from –II to +VI), the principal being II (d^6) and III (d^5). A number of iron-dependent monooxygenases are able to generate high-valent Fe(IV) or Fe(V) reactive intermediates during their catalytic cycle. Whereas, Fe^{2+} is extremely water-soluble, Fe^{3+} is quite insoluble in water ($K_{sp} = 10^{-39}$ M and at pH 7.0, $[Fe^{3+}] = 10^{-18}$ M) and significant concentrations of water-soluble Fe^{3+} species can be attained only by strong complex formation with appropriate ligands.

The interaction between Fe^{2+} and Fe^{3+} and ligand donor atoms will depend on the strength of the chemical bond formed between them. An idea of the strength of such bonds can be found in the concept of 'hard' and 'soft' acids and bases (HSAB) (Pearson, 1963). 'Soft' bases have donor atoms of high polarisability with empty, low-energy orbitals; they usually have low electronegativity and are easily oxidised. In contrast, 'hard' bases have donor atoms of low polarisability, and only have vacant orbitals of high energy; they have high electronegativity and are difficult to oxidise. Metal ions are 'soft' acids if they are of low charge density, have a large ionic radius. and have easily excited outer electrons. 'Hard' acid metal ions have high charge density, a small ionic radius, and no easily excited outer electrons. In general, 'hard' acids prefer 'hard' bases and 'soft' acids form more stable complexes with 'soft' bases (Pearson, 1963). Fe(III) with an ionic radius of 0.067 nm and a charge of 3^+ is a 'hard' acid and will prefer 'hard' oxygen ligands such as phenolate and carboxylate, compared to imidazole or thiolate. In contrast, Fe(II) with an ionic radius of

0.083 nm and a charge of only 2^+ is on the borderline between 'hard' and 'soft,' favouring nitrogen (imidazole and pyrrole) and sulphur ligands (thiolate and methionine) over oxygen ligands.

The coordination number of 6 is the most frequently found for both Fe(II) and Fe(III) giving octahedral stereochemistry, although four-coordinate (tetrahedral) and particularly five-coordinate complexes (trigonal bipyramidal or square pyrimidal) are also found. For octahedral complexes, two different spin states[1] can be observed. Strong-field ligands (e.g. Fe^{3+} OH^-), where the crystal field splitting is high and hence electrons are paired, give low-spin complexes, while weak-field ligands (e.g. CO, CN^-), where crystal field splitting is low, favour a maximum number of unpaired electrons and give high-spin complexes Changes of spin state affect the ion size of both Fe(II) and Fe(III), the high-spin ion being significantly larger than the low-spin ion. As we will see in Chapter 2, this is put to good use as a trigger for the cooperative binding of dioxygen to haemoglobin. High-spin complexes are kinetically labile, while low-spin complexes are exchange-inert. For both oxidation states only high-spin tetrahedral complexes are formed, and both oxidation states are Lewis acids, particularly the ferric state.

The unique biological role of iron comes from the extreme variability of the Fe^{2+}/Fe^{3+} redox potential, which can be fine-tuned by well-chosen ligands, so that iron sites can encompass almost the entire biologically significant range of redox potentials, from about –0.5 V to about +0.6 V. However, as we will see in Chapter 13, copper allows access to an even higher range of redox potentials (0 V to +0.8 V), which turned out to be of crucial importance in the Earth's rapidly evolving aerobic environment, following the arrival of water-splitting, oxygen-generating photosynthetic organisms.

1.2 Interactions of Iron with Dioxygen and Chemistry of Oxygen Free Radicals

Molecular oxygen was not present when life began on Earth, with its essentially reducing atmosphere, and both the natural abundance of iron and its redox properties predisposed it to play a crucial role in the first stages of life on Earth. About one billion (10^9) years ago, photosynthetic prokaryotes (Cyanobacteria) appeared and dioxygen was evolved into the Earth's atmosphere. It probably required 200–300 million years – a relatively short time on a geological time scale – for oxygen to attain a significant concentration in the atmosphere, since at the outset the oxygen produced by photosynthesis would have been consumed by the oxidation of ferrous ions in the oceans. Once dioxygen had become a dominant chemical entity, iron hydroxides precipitated, as the Precambrian deposits of red ferric oxides laid down in the geological strata at that time bear witness. Concomitant with the loss of iron bioavailability, the oxidation of Cu(I) led to soluble Cu(II). While enzymes active in anaerobic metabolism were designed to be active in the lower portion of the redox potential spectrum, the presence of dioxygen created the need for a new redox active metal with $E_o M^{n+1}/M^n$ from 0 to 0.8 V. Copper, now bioavailable (Crichton and Pierre, 2001), was ideally suited for this role and began to be used in enzymes with higher redox potentials (as a di-copper centre in laccase and a mixed iron-copper centre in cytochrome oxidase) to take advantage of the oxidizing power of dioxygen. Some typical redox potentials for iron and copper proteins and chelates are given in Figure 1.1.

Although oxygen must ultimately completely oxidise all biological matter, its propensity for biological oxidation is considerably slowed by the fact that in its ground state (lowest energy state)

---

[1] The spin state is defined as the orientation in a strong magnetic field of an unpaired electron (or a nuclear spin), i.e. either parallel or antiparallel to the direction of the magnetic field.
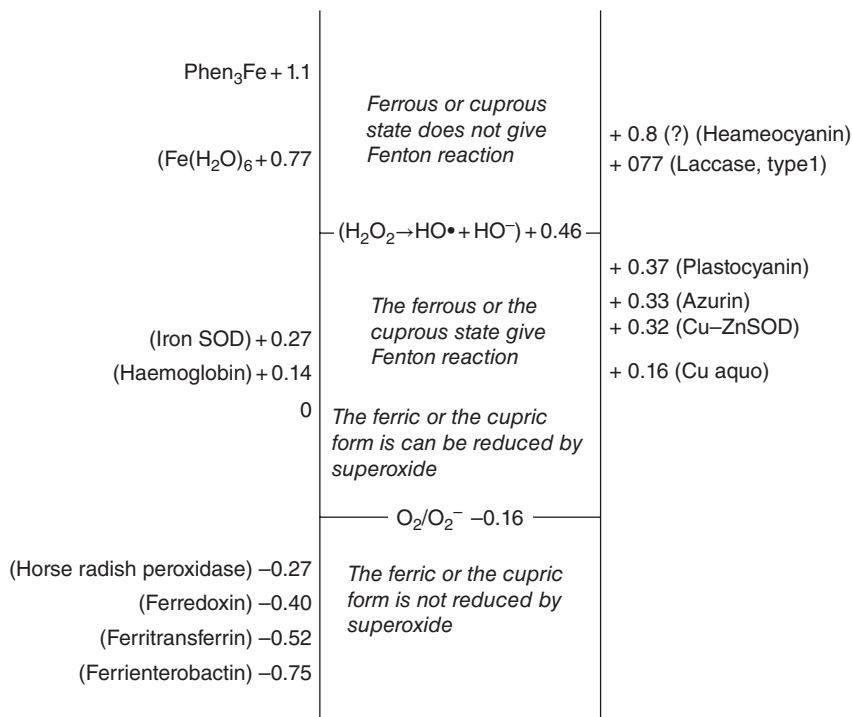
Phen$_3$Fe + 1.1

(Fe(H$_2$O)$_6$ + 0.77

Ferrous or cuprous state does not give Fenton reaction

+ 0.8 (?) (Heameocyanin)
+ 077 (Laccase, type1)

— (H$_2$O$_2$→HO• + HO$^-$) + 0.46 —

+ 0.37 (Plastocyanin)
+ 0.33 (Azurin)
+ 0.32 (Cu–ZnSOD)

The ferrous or the cuprous state give Fenton reaction

(Iron SOD) + 0.27
(Haemoglobin) + 0.14

+ 0.16 (Cu aquo)

0

The ferric or the cupric form is can be reduced by superoxide

— O$_2$/O$_2^-$ −0.16 —

(Horse radish peroxidase) −0.27
(Ferredoxin) −0.40
(Ferritransferrin) −0.52
(Ferrienterobactin) −0.75

The ferric or the cupric form is not reduced by superoxide

Figure 1.1 *Some redox potentials (in Volts) of iron and copper enzymes and chelates at pH 7 relative to the standard hydrogen electrode. Figure reproduced with permission from Crichton and Pierre (2001)*

it exists as a triplet spin state, whereas most biological molecules are in the singlet state as their lowest energy level. Spin inversion is relatively slow, so that oxygen reacts much more easily with other triplet state molecules or with free radicals than with singlet state molecules.

The arrangement of electrons in most atoms and molecules is such that they occur in pairs, each of which have opposite intrinsic spin angular momentum. Molecules which have one or more unpaired electrons are termed free-radicals: these are generally very reactive and will act as chain carriers in chemical reactions. Thus, the hydrogen atom, with one unpaired electron, is a free radical, as are most transition metals and the oxygen molecule itself. The dioxygen molecule has two unpaired electrons, each located in a different π^* anti-bonding orbital. Since these two electrons have the same spin quantum number, if the oxygen molecule attempts to oxidise another atom or molecule by accepting a pair of electrons from it, both new electrons must have parallel spins in order to fit into the vacant spaces in the π^* orbitals. A pair of electrons in an atomic or molecular orbital would have anti-parallel spins (of $+\frac{1}{2}$ and $-\frac{1}{2}$) in accordance with Pauli's principle. This imposes a restriction on oxidation by O_2, which means that dioxygen tends to accept its electrons one at a time and slows its reaction with non-radical species (Halliwell and Gutteridge, 1984). Transition metals can overcome this spin restriction on account of their ability to accept and donate single electrons. The interaction of iron centres and oxygen is of paramount importance in biological inorganic chemistry, and some of the main features have been summarised in Figure 1.2.

The reactivity of O_2 can be increased in another way, by moving one of the unpaired electrons in a way that alleviates the spin restriction to give the two singlet states of O_2. The most important of the two forms of singlet $O_2^1\delta_g$ in biological systems has no unpaired electrons, is not a radical,
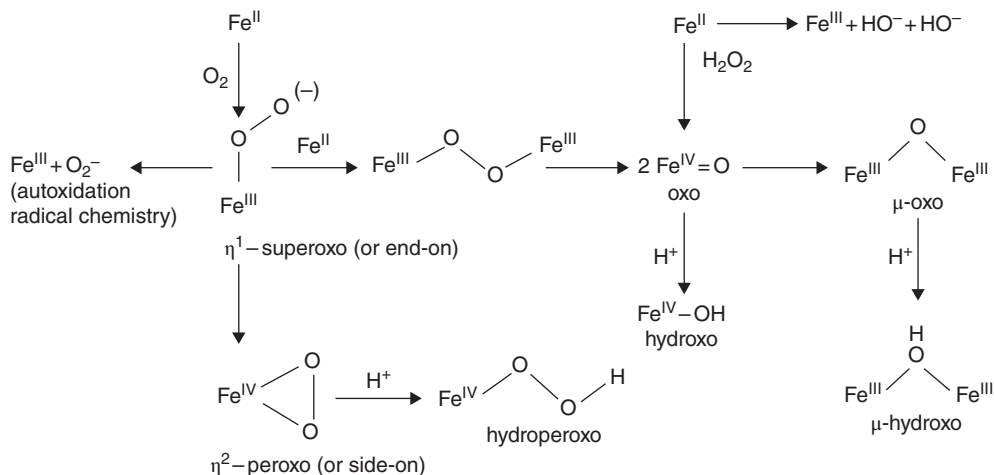
Figure 1.2 *Iron–oxygen chemistry. Multibridged species have been omitted. Figure reproduced with permission from Crichton and Pierre (2001)*

and can be obtained when a number of biological pigments such as chlorophylls, retinal, flavins or porphyrins are illuminated in the presence of O_2. When a single electron is accepted by the ground-state O_2 molecule, it must enter one of the π^* anti-bonding orbitals, to form the superoxide radical, O_2^-. The addition of a second electron to O_2^- gives the peroxide ion O_2^{2-} with no unpaired electrons. At physiological pH, O_2^{2-} will immediately protonate to give hydrogen peroxide, H_2O_2. The third reactive oxygen species found in biological system is the hydroxyl free radical. Two hydroxyl radicals, ·OH can be formed by homolytic fission of the O–O bond in H_2O_2, either by heating or by irradiation. However, as Fenton first observed in 1894 (Fenton, 1894), a simple mixture of H_2O_2 and an Fe(II) salt also produces the ·OH radical (Eq. 1.1):

$$Fe^{2+} + H_2O_2 \rightarrow \quad Fe^{3+} + \bullet OH + OH^- \tag{1.1}$$
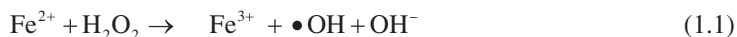
In the presence of trace amounts of iron, superoxide can then reduce Fe^{3+} to molecular oxygen and Fe^{2+}. The sum of this reaction (Eq. 1.2), plus the Fenton reaction (Eq. 1.1), produces molecular oxygen, hydroxyl radical and hydroxyl anion from superoxide and hydrogen peroxide, in the presence of catalytic amounts of iron – the so-called Haber–Weiss[2] reaction (Eq. 1.3) (Haber and Weiss, 1934).

$$Fe^{3+} + O_2^- \rightarrow Fe^{2+} + O_2 \tag{1.2}$$

$$O_2^- + H_2O_2 \rightarrow O_2 + \bullet OH + OH^- \tag{1.3}$$

Iron or copper complexes will catalyse Fenton chemistry only if two conditions are met simultaneously, namely that the ferric complex can be reduced and that the ferrous complex has an oxidation potential such that it can transfer an electron to H_2O_2. However, it must also be added that this reasoning supposes that standard conditions are present and at equilibrium, which is rarely the case

---

[2] The reaction was originally described by Haber and Wilstätter (1931), but the original paper was published in German! The more frequently cited Haber and Weiss paper does cite the original, but in neither is a reference to Fenton given.

for biological systems. A simple example will illustrate the problem: whereas, under standard conditions reaction (1.2) has a redox potential of –330 mV (at an O_2 concentration of 1 atmosphere), *in vivo* with $[O_2] = 3.5 \times 10^{-5}$ M and $[O_2^-] = 10^{-11}$ M the redox potential is +230 mV (Pierre and Fontecave, 1999).

In aqueous solution in the absence of oxygen, iron is present as the hydrated hexa-aqua ferrous II ion, $Fe(H_2O)_6^{2+}$. In the early stages of evolution the atmosphere was thought to be essentially reducing with a very low oxygen pressure, and thus a high concentration of reduced iron would have been present. The appearance of molecular oxygen, which accompanied the arrival of photosynthetic organisms capable of the fixation of atmospheric carbon dioxide with concomitant water splitting to yield electrons, protons and oxygen, changed the situation dramatically, since the following reaction (Eq. 1.4) (here simplified by neglecting the hydration of the ferrous ion) would result:

$$Fe(II)aq + O_2 \rightarrow Fe(III)aq + O_{2-} \qquad (1.4)$$
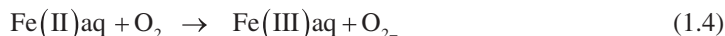
Except at very low pH values, the hexa-aqua ferric ion, $Fe(H_2O)_6^{3+}$, would then undergo a series of hydrolysis and polymerisation reactions leading progressively to more and more insoluble ferric polynuclears. These would then precipitate to provide geologic evidence of the oxygenation of the atmosphere by the presence around the mid Precambrian of intense red deposits of ferric oxides. The inorganic chemistry involved in these processes is becoming better understood (Jolivet *et al.*, 2004), and the remainder of this chapter is concerned with the pathways of iron hydrolysis and polymerisation, and concludes with some thoughts on biomineralisation.

1.3 Hydrolysis of Iron Salts

Iron salts have a strong predisposition to hydrolyze in aqueous solutions, in a complex process involving the following steps (Flynn, 1984): (i) an initial hydrolysis with the formation of soluble low-molecular-weight complexes; (ii) the formation and ageing of polynuclear clusters; and finally (iii) the precipitation of insoluble Fe(III) oxides and hydroxides. At low pH, iron typically forms hexacoordinated aquo complexes, $[Fe(H_2O)_6]^{z+}$, in which polarisation of the coordinated water molecules will depend on the oxidation state and the size of the cation. Ferric aquo complexes are more acidic than ferrous, and hydroxylation of the cations occurs in very distinct ranges of pH, as can be seen from the speciation diagram (Figure 1.3).

Hydrolysis originates from the loss of protons from the aqua metal ion – going from $[Fe(OH)_h Fe(H_2O)_{6-h}]^{(z-h)+}$, where $h = 0$, with progressively increasing values of h, with each step accompanied by the release of H^+. The first step for ferric iron is shown in the reaction (Eq. 1.5):

$$\left[Fe(H_2O)_6\right]^{3+} \rightleftarrows \left[Fe(H_2O)_5(OH)\right]^{2+} + H^+ \qquad (1.5)$$
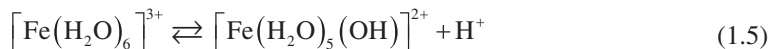
Between pH 5 and pH 9, which is clearly of relevance to living organisms as well as aquatic systems, ferric salts hydrolyze immediately whereas ferrous salts, in the absence of oxygen or other oxidizing agents, give solutions of ferrous aqua ions, $Fe(H_2O)_6^{2+}$. Thus, in biological media the hydrated ferrous ion is a real species (Figure 1.3), whereas the hydrated ferric ion is relatively rare (Jolivet *et al.*, 2004), although significant concentrations of $Fe(H_2O)_6^{3+}$ are present at very low pH values. In most lakes, estuaries, streams and rivers, iron levels are high and Fe^{2+} is produced by the photolysis of inner-sphere complexes of particulate and colloidal iron(III) hydroxides with biogenic organic ligands. Since the photic zones in which this takes place are aerobic, there is continuous
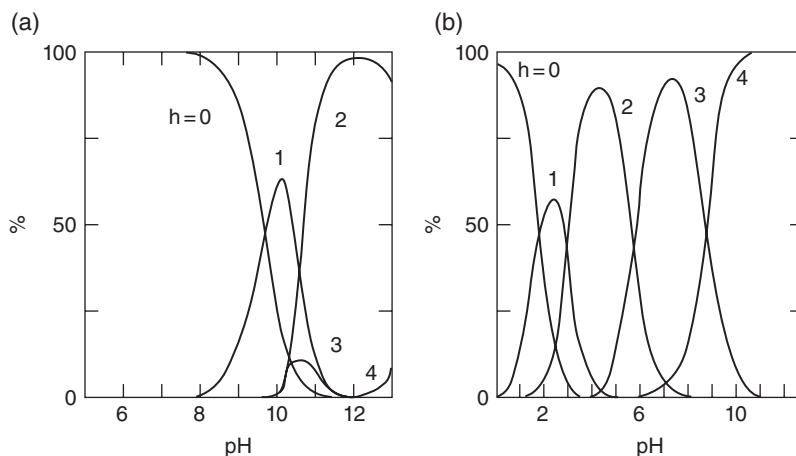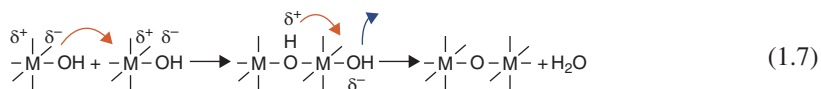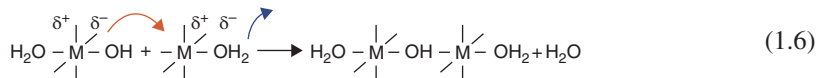
Figure 1.3 *Speciation of $[Fe(OH)_h(H_2O)_{6-h}]^{(z-h)+}$ complexes of (a) Fe(II); (b) Fe(III). From Jolivet* et al. *(2004)*

reoxidation of iron, producing secondary colloidal iron(III) hydroxides. In deeper waters, settling organic matter can supply reducing equivalents to convert FeO·OH to Fe^{2+}. In contrast, iron levels in surface seawater are extremely low, ranging from 0.02 to 1 nM (Wu and Luther, 1996).

Hydroxylated complexes can condense by the elimination of water and formation of μ-hydroxo bridges (olation) (Eq. 1.6), whereas oxohydroxy complexes – where there is no water molecule – condense in a two-step mechanism leading to the formation of μ-oxo bridges (oxolation) (Eq. 1.7):

$$H_2O - \overset{|}{\underset{|}{M}} - OH + - \overset{|}{\underset{|}{M}} - OH_2 \longrightarrow H_2O - \overset{|}{\underset{|}{M}} - OH - \overset{|}{\underset{|}{M}} - OH_2 + H_2O \qquad (1.6)$$

$$- \overset{|}{\underset{|}{M}} - OH + - \overset{|}{\underset{|}{M}} - OH \longrightarrow - \overset{|}{\underset{|}{M}} - O - \overset{|}{\underset{|}{M}} - OH \longrightarrow - \overset{|}{\underset{|}{M}} - O - \overset{|}{\underset{|}{M}} - + H_2O \qquad (1.7)$$

For ferric complexes, condensation occurs from strongly acidic media (pH ~1), whereas ferrous complexes condense only above pH 6, and the formation of polycationic ferrous species is poorly documented. Ferrous ions under anaerobic conditions can be hydroxylated from the $[Fe(OH)_2Fe(H_2O)_4]^0$ stage at pH > 6–7, leading to the precipitation of $Fe(OH)_2$. The reaction pathway for the formation of $Fe(OH)_2$, as shown in Figure 1.4, involves the olation of $[Fe_2(OH)_2(H_2O)_8]^{2+}$ dimers to planar tetramers $[Fe_4(OH)_8(H_2O)_8]^0$, followed by the rapid growth of nuclei in the same plane and resulting in the layered brucite structure [typical of hydroxides of divalent metal ions – brucite is the mineral form of magnesium hydroxide, $Mg(OH)_2$]. Both, in the solid state or in aqueous solutions, ferrous phases are extremely sensitive to oxidation, forming mixed ferric–ferrous products (green rusts, magnetite, goethite, lepidocrocite). The rapid oxidation of $Fe(OH)_2$ at pH 7 represents a unique way to form lepidocrocite, γ-FeO·OH, which is isostructural with the aluminium oxide hydroxide, boehmite, γ-AlO·OH.

The hydrolysis of ferric solutions is readily induced by the addition of base. Upon the addition of base at a rather acid pH, the purple ferric aqua-ion $Fe(H_2O)_6^{3+}$ initially undergoes a first

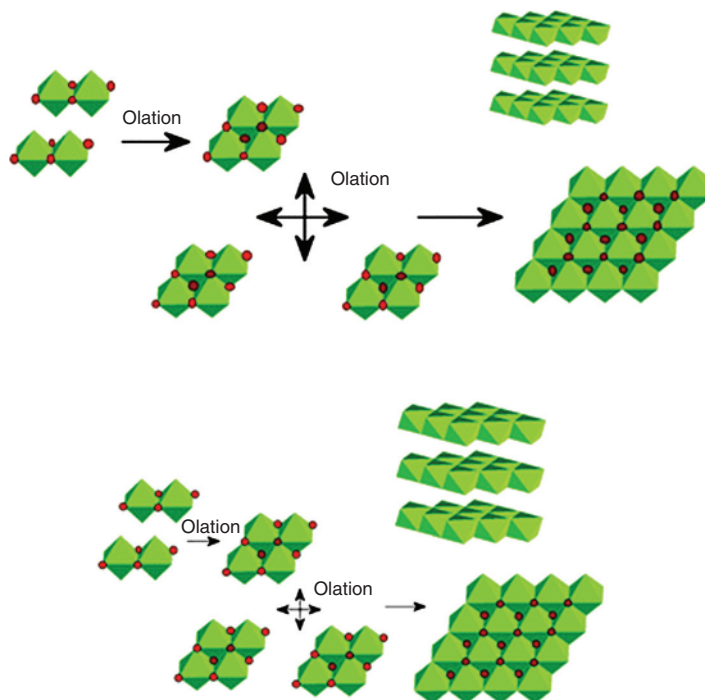***Figure 1.4*** *A possible reaction pathway for the formation of Fe(OH)$_2$. From Jolivet* et al. *(2004)*

deprotonation step, which is followed by reversible dimerisation, giving a yellow solution of mono-and dinuclear species. The equilibria leading to mono- and dinuclear hydrolysis products such as $[FeOH]^{2+}$, $[Fe(OH)_2]^+$ and $[Fe_2(OH)_2]^{4+}$ are established rapidly and are well understood (Cornell *et al*., 1989). These low-molecular species interact to produce hydrolytic polymers such as $[Fe_p(OH)_r(H_2O)_s]^{(3-r)+}$, or $[Fe_pO_r(OH)_s]^{(3p-2r-s)+}$ and precipitated oxides such as $Fe(OH)_3$, $FeO \cdot OH$ and Fe_2O_3 (Feng and Nansheng, 2000; Flynn, 1984; Schwertmann *et al*., 1999).

On account of their high reactivity, ferric complexes condense very rapidly, and the process is difficult to stop without the use of very strongly complexing polydentate ligands. However, a range of species containing polynuclear Fe(III) cores have been characterised using a number of polycarboxylate or amino ligands (Lippard, 1988; Taft and Lippard, 1990; Taft *et al*., 1993; Schmitt *et al*., 2001; Jones *et al*., 2002; Hellman *et al*., 2006), two of which are illustrated in Figure 1.5.

1.4   Formation and Characterisation of Ferrihydrite

The addition of base to solutions of ferric ions at pH values >3 immediately leads to the precipitation of a poorly ordered, amorphous, red-brown ferric hydroxide precipitate. This synthetic precipitate resembles ferrihydrite, a hydrous ferric oxyhydroxide mineral found in many near-surface soils and sediments (Rancourt *et al*., 2001; Schwertmann *et al*., 1987), and is also present in the iron oxyhydroxide core of the iron storage protein, ferritin (see Chapter 6). Ferrihydrite can be considered as the least stable but most reactive form of iron(III), the group name for amorphous phases with large specific surface areas ($>340\,m^2\,g^{-1}$). The presence of ferrihydrite is often
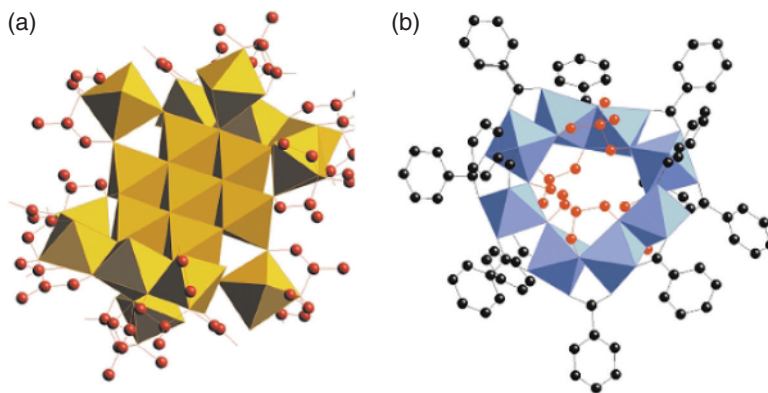
Figure 1.5 *Examples of polycationic structures formed by ferric ions in the presence of strongly complexing ligands. (a) $[Fe_{19}O_6(OH)_{14}(L)^{10}(H_2O)_{12}]^+$ $L = N(CH_2COOH)_2(CH_2CH_2OH)$; (b) $Fe_8(PhCOO)_{12}(thme)_4 \cdot 2Et_2O$ (thme: tris-hydroxymethylethane). From Jolivet* et al. *(2004)*

underestimated because of difficulties in its definitive identification and also because of its common designation (covering a range of poorly ordered compounds), such as amorphous iron hydroxide, colloidal ferric hydroxide, $Fe(OH)_3$.

Ferrihydrite has been identified as a preterrestrial component of meteorites, and may be a constituent of the soils of Mars (Bishop *et al.*, 1995). On Earth, ferrihydrite is ubiquitous in natural waters, in the sediments derived from these waters, and is a constituent of a wide variety of soils, particularly those formed under cool and moist conditions as the precursor of hematite. It is also abundantly present in the precipitates resulting from acid mine drainage. Its high surface area and reactivity enable it to sequester a number of species through absorption, coprecipitation and redox reactions (Fortin and Langley, 2005). Because of its extremely high surface area and reactivity, ferrihydrite is manufactured for a variety of industrial applications (Li *et al.*, 2011), including coal liquefaction and metallurgical processing (Huffman *et al.*, 1993; Riveros *et al.*, 2001), and as an effective heavy metal scavenger in wastewater treatments (Ford *et al.*, 1997).

The conventional classification of ferrihydrite is based on the number of X-ray diffraction (XRD) peaks. Normally, a distinction is drawn between two types of ferrihydrite, referred to as '2-line ferrihydrite,' which describes a material that exhibits little crystallinity, and '6-line ferrihydrite,' which has the best crystallinity. In a typical XRD pattern of these materials, the 2-line form displays two broad peaks at 1.5 and 2.5 Å, while the more crystalline 6-line form displays six peaks at 1.5 (a doublet), 1.7, 2.0, 2.2, and 2.5 Å (Jambor and Dutrizac, 1998). The degree of order found in synthetic ferrihydrite depends on the method of preparation and the time of its ageing, which requires careful control of pH, temperature and concentration. The brief heating of Fe(III) solutions to about 80 °C typically produces '6-line ferrihydrite,' whereas the 2-line variety is typically produced at ambient temperatures by the addition of alkali to raise the pH to about 7. It seems to be agreed that ferrihydrite is not amorphous and has at least some degree of crystallinity. Despite the ease of its synthesis in the laboratory, no single formula is widely accepted, and compositions ranging from $Fe_5HO_8 \cdot 4H_2O$ (Towe and Bradley, 1967), through $5Fe_2O_3 \cdot 9H_2O$ (Towe, 1981) and $Fe_{10}O_{14}(OH)_2$ (Michel *et al.*, 2007a) to the recent $Fe_{8.2}O_{8.5}(OH)_{7.4} + 3H_2O$ (Michel *et al.*, 2010) have been proposed. It has been demonstrated that almost all of the water can be replaced by adsorbed species in quantities that cannot be accommodated within the crystal structure, and it was proposed that the bulk structural unit for ferrihydrite is an $Fe(O,OH)_6$ octahedron, where the surface
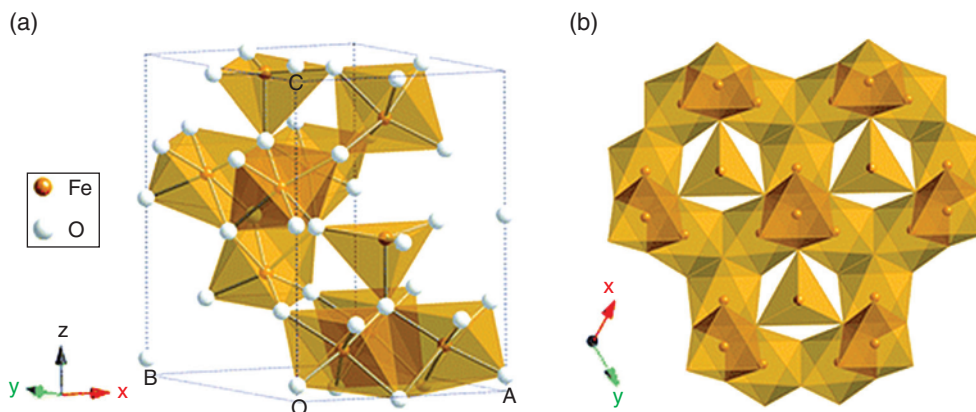
(a)

(b)

Figure 1.6 *Ferrihydrite structure. (a) Unit cell and (b) basic motif of the ferrihydrite model proposed by Michel* et al.*, 2007. From Smith* et al. *(2012)*

structure is a mixture of octahedrally and tetrahedrally coordinated Fe (Jambor and Dutrizac, 1998). These 'coordination–unsaturated' surface sites are readily accessible to the adsorption of foreign species and, together with the large surface area referred to above, most likely account for the high adsorptive capacity of ferrihydrite.

While it is considered to be a good example of a nanomineral (Hochella *et al.*, 2008), the crystal structure (Jambor and Dutrizac, 1998; Manceau, 2009; Michel *et al.*, 2007a; Rancourt and Meunier, 2008), physical (Rancourt and Meunier, 2008; Hiemstra and Van Rielsdijk, 2009) and magnetic (Coey and Readman, 1973; Pankhurst and Pollard, 1992; Pannalai *et al.*, 2005; Berquo *et al.*, 2007, 2009; Cabello *et al.*, 2009) properties of ferrihydrite remain controversial. Over the years, a number of structural models have been proposed for ferrihydrite (reviewed in Jambor and Dutrizac, 1998). Towe and Bradley (1967) and Chukrov *et al.* (1974) both proposed what were essentially defective hematite structures, whereas Drits *et al.* (1993) proposed a multicomponent model consisting of defective and defect-free ferrihydrite phases mixed with ultradisperse hematite. Unlike other iron hydroxides which have been studied, the exact structure and chemical composition of ferrihydrite has remained a matter of considerable debate, and until recently there has been no consensus on its crystal structure. Most of the disagreement has centred around the presence of multiple structural phases and the local environment of the iron (Drits *et al.*, 1993; Janney *et al.*, 2000, 2001; Jansen *et al.*, 2002).

Recent X-ray scattering studies from both 2-line and 6-line ferrihydrite suggest that the coherent scattering domains share a common structure, despite the fact that the average crystallite size and water content were different (Michel *et al.*, 2007b). An atomic arrangement of ferrihydrite (Figure 1.6) has been proposed (Michel *et al.*, 2007a) using the pair-distribution function (PDF) method for structural analysis, which involves a comparison between PDFs generated from the experimental X-ray scattering data with those calculated from structural models (Billinge and Kanatzidis, 2004). On the basis of their results, these authors concluded that in its ideal form, the structure contains 20% tetrahedrally and 80% octahedrally coordinated iron, and has a basic structural motif closely related to the Baker–Figgis–δ-Keggin cluster[3] (Casey, 2006).

---

[3] The Baker–Figgis–Keggin isomers (of which there are five, from α to ε) are aluminium hydroxide clusters which have central metals tetrahedrally coordinated to oxygen $[M(O)_4]$ sites, and are familiar structures among scientists who study polyoxometalates. They form aluminium clusters with the stoichiometry $MO_4Al_{12}(OH)_{24}(H_2O)_{12}^{7+}$(aq) [M = Ge(IV), Ga(III), or Al(III)].

The compositional, structural, and magnetic changes that occur upon aging of '2-line' ferrihydrite in the presence of adsorbed citrate at elevated temperature has been studied more recently (Michel *et al*., 2010). Whereas, aging under these conditions ultimately results in the formation of hematite, analysis of the atomic pair distribution function and complementary physico-chemical and magnetic data indicate the formation of an intermediate ferrihydrite phase of larger particle size with few defects, more structural relaxation and electron spin ordering, and pronounced ferrimagnetism relative to its disordered ferrihydrite precursor. The results validate the previously proposed structural model (Michel *et al*., 2007a) and identify a pathway for forming ferrimagnetic ferrihydrite which might explain the magnetic enhancement that typically precedes the formation of hematite in aerobic soil and weathering environments. The 20:80 ratio of tetrahedral to octahedral Fe sites proposed is supported by XANES/EXAFS studies (Carta *et al*., 2009; Maillot *et al*., 2011), and a new synthetic route to chemically pure 2-line ferrihydrite (Smith *et al*., 2012) confirms that the structure of ferrihydrite is consistent, repeatable, regardless of the synthetic method used, the water content or particle size of the crystallites, and is adequately described by the hexagonal model.

1.5   Ageing of Amorphous Ferrihydrite to more Crystalline Products

Ferrihydrite is thermodynamically unstable and transforms with time into the more stable crystalline oxides hematite and goethite (Figure 1.7). Between pH 5 and 8, on account of the poor solubility of ferrihydrite ($\sim 10^{-10}$ M), the transformation can only proceed by *in situ* dehydration and local rearrangement, resulting in very small crystallites of hematite, $\alpha\text{-Fe}_2\text{O}_3$. When the solubility of ferrihydrite is higher (pH <4 or >8), transformation can proceed by a dissolution/crystallisation pathway, leading to goethite, $\alpha\text{-FeOOH}$ (Figure 1.7). The thermolysis of acidic solutions (pH <3) of ferrihydrite at 90–100 °C leads to hematite (Jolivet, 2000). The presence of adsorbed species can drastically increase the transformation temperature, as illustrated by the observation that an Si/Fe ratio of 0.25 in ferrihydrite increases the temperature required to convert ferrihydrite to hematite to 800 °C. This effect of complexing ligands such as silicate, and particularly phosphate, in delaying or preventing the transformation of ferrihydrite into crystalline mineral phases, may explain the presence of ferrihydrite both in very old soils and in the mineral core of mammalian ferritins (Jolivet *et al*., 2004).

The presence of both ferrous and ferric ions in solutions orients the condensation presence to the formation of specific phases, namely green rusts and spinel-type magnetite (or maghemite). The type of product formed depends on many factors, including pH, and particularly the composition of the system, defined as $x = \text{Fe}^{3+}(\text{Fe}^{2+} + \text{Fe}^{3+})$ (Figure 1.8). For x <0.66 and $\text{OH}^-/\text{Fe}_{total} = 2$ (pH 8), hydroxylation of the mixture gives green rusts, in which the Fe^{2+} and Fe^{3+} ions occupy octahedral sites giving a positive charge to the sheet-like structure, which is balanced by the intercalation of anions. When tetrahedral anions such as sulphate are present, the 'green rust SO_4' has the unique composition, Fe(II)/Fe(III) = 2 (Refait *et al*., 1998; Géhin *et al*., 2002).

In contrast, magnetite Fe_3O_4 can be easily obtained (Figure 1.8) by coprecipitating aqueous Fe^{2+} and Fe^{3+} ions with $x = 0.66$. The iron atoms are distributed in the octahedral (Oh) and tetrahedral (Td) sites of the face-centred cube of oxygen according to ($[\text{Fe}^{3+}]_{Td}[\text{Fe}^{2+}\text{Fe}^{3+}]_{Oh}\text{O}_4$). Magnetite is characterised by rapid electron hopping between the iron cations in the octahedral sublattice, and during the quasi-immediate crystallisation of the spinel at room temperature, electron transfer between Fe^{2+} and Fe^{3+} ions plays a fundamental role in the process (Jolivet *et al*., 2004).
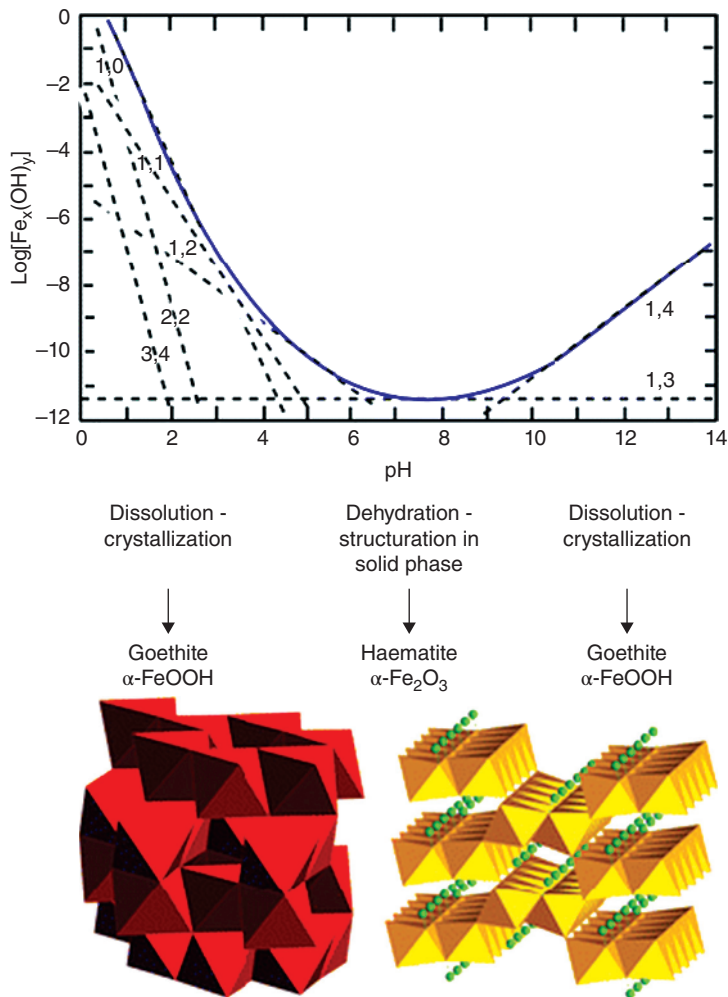
Figure 1.7 *Influence of pH on the solubility of iron and ferric (hydro)oxide crystal structures. From Jolivet* et al. *(2004)*

1.6 Biomineralisation

The most obvious product of biomineralisation is the calcium phosphate of vertebrate teeth and bones, but others include calcium in the shells of marine organisms, silicon in grasses, and the calcium carbonate shells of molluscs. Biomineralisation involves the formation of these inorganic materials under the influence of proteins, carbohydrates and lipids. The way in which biominerals grow is intimately linked to the problem of morphology, and it is difficult to think of a better introduction to this field than the pioneering work of D'Arcy Thompson.

D'Arcy Wentworth Thompson (1860–1948) was a polymath, equally well qualified to occupy chairs of Zoology, Mathematics and Physics, but chose the former in Dundee and then St Andrews, and was a pioneer of bio-mathematics. His classic book '*On growth and form*' is essentially about

Figure 1.8 *Representation of the phases formed in solution as a function of the composition and hydroxylation ratio in the ferrous–ferric system. From Jolivet* et al. *(2004)*

biominerals (Thompson, 1917). This fascinating problem includes the initiation of nucleation, growth of the inorganic crystalline phases, and definition of the volume and shape of the inorganic material, which is determined by the organic mould (lipid, protein, carbohydrate) within which the inorganic mineral structure is deposited (reviewed in Mann, 2007; Bäuerlein, 2000; Wilt 2005; Nudelman and Sommerdijk, 2012).

There are 14 iron oxides, hydroxides and oxyhydroxides that have been more or less well-defined, 10 of which are known to occur in Nature (Table 1.1). Of these, goethite, hematite and

Table 1.1 *Oxides, hydroxides and oxyhydroxides of iron*

Mineral	Nominal formula	Phase	Nominal formula
Goethite	α-FeOOH	synthetic	$Fe(OH)_2$
Akaganéite	β-FeOOH	synthetic	β-Fe_2O_3
Lepidocrocite	γ-FeOOH	synthetic	ε-Fe_2O_3
Feroxyhite	δ-FeOOH	synthetic	FeOOH
Hematite	α-Fe_2O_3		
Maghemite	γ-Fe_2O_3		
Magnetite	Fe_3O_4		
Wüstite	FeO		
Bernalite	$Fe(OH)_3$		
Ferrihydrite	$Fe_5HO_8 \cdot 4H_2O$/ $5Fe_2O_3 \cdot 9H_2O$/ $Fe_{10}O_{14}(OH)_2$		

Adapted with permission from Jambor, J.L. and Dutrizac, J.E. (1998) Occurrence and constitution of natural and synthetic ferrihydrite, a widespread iron oxyhydroxide. *Chem. Rev.,* **98**, 2549–2585; © 1998, American Chemical Society.

Table 1.2 *Diagnostic criteria for iron oxide minerals*

Mineral	Colour	Most intense X-ray lines (Å)	IR bands (cm^{-1})	Magnetic hyperfine field (T)		
				295 °K	77 °K	4 °K
Ferrihydrite	Reddish brown	2.54, 2.24, 1.97, 1.73, 1.47		–	–	47–50
Hematite	Bright red	2.70, 3.68, 2.52	345, 470, 540	51.8	54.2/53.5	54.2/53.5
Maghemite	Red to brown	2.52, 2.95	400, 450, 570, 590, 630	50	–	52.6
Magnetite	Black	2.53, 2.97		49.1/46.0	–	–
Goethite	Yellowish brown	4.18, 2.45, 2.69	400, 590	38.2	50.3	
Lepidocrocite	Orange	6.26, 3.29, 2.47, 1.937	890, 797 1026, 1161, 753	–	–	45.8
Akaganéite	Yellowish brown	3.33, 2.55, 7.47	840, 640	–	47.1, 46.7, 45.3	48.9, 47.8, 47.3
Feroxyhyte	Reddish brown	2.54, 2.22, 1.69, 1.47	1110, 920, 790, 670	42.0	53.0	53.5
Bernalite	Dark green	3.784, 1.682, 2.393, 2.676, 1.892		42.0		55.7

magnetite occur in sufficient abundance to be considered as rock-forming minerals. Lepidocrocite, ferrihydrite and maghemite are found in sediments from many localities, but they all occur much less frequently and in much lower abundance than goethite, hematite and magnetite. The diagnostic criteria for each of these iron oxides are listed in Table 1.2.

The biomineralisation of a number of iron oxide minerals has been studied. The oxy-hydroxide phase ferrihydrite (as discussed above) constitutes the central core of the iron storage protein ferritin, and its biomineralisation will be considered in greater detail in Chapter 6. Goethite (α-FeOOH) is biomineralised by limpets, and lepidocrocite (γ-FeOOH) by chitons (Mann, 1988), while magnetite (Fe_3O_4) is found in the magnetosomes of magnetotactic bacteria (Blakemore, 1975) and also in vertebrates (Kirschvink *et al*., 2001).

1.7   Magnetite Biomineralisation by Magnetotactic Bacteria

Aquatic bacteria exhibiting magnetotaxis – that is, orienting and migrating along geomagnetic field lines – were discovered serendipitously in the mid 1970s.[4] This ability is dependent on the formation of intracellular magnetic structures, magnetosomes, which allow magnetotactic bacteria to orient in external magnetic fields. The magnetosome consists of a chain of nanometre-sized,

---

[4] At the Marine Station at Woods Hole, Massachusetts, Richard Blakemore observed that bacteria from marine and freshwater muds accumulated at the North side of drops of water and sediment, when placed upon a microscope slide, and that these bacteria swam towards and away from the south and north pole of a bar magnet, respectively (Blakemore, 1975). He subsequently showed that such magnetotactic bacteria behave like self-propelled, permanent magnetic dipole moments. Magnetotactic bacteria use magnetite (Fe_3O_4) as an internal compass with which to navigate, and in the Northern hemisphere their magnetic dipole is oriented northward, whereas magnetotactic bacteria from the Southern hemisphere have their dipole oriented southward. These microorganisms, isolated in the Northern hemisphere, swim northwards and downwards along the Earth's magnetic field lines, to avoid the higher oxygen concentrations of surface water, which are toxic to them. If transferred to the Southern hemisphere they '*perd leur Nord*', and swim upward!

membrane-bound crystals of the magnetic iron minerals magnetite (Fe_3O_4) or, less frequently, greignite (Fe_3S_4) (Figure 1.9). Magnetotactic bacteria (MTB) are found in a variety of freshwater and marine aquatic environments and belong to a wide range of phylogenetic groups. The most commonly studied MTB have a single magnetosome chain consisting of 15–20 crystals of magnetite each ~50 nm in diameter, although a considerable diversity in magnetosome morphologies has been found within the rich diversity of MTB. For an historical perspective of the discovery and early studies on the ecological distribution of MTB the reader is referred to the article by Blakemore (1982), while more recent reviews can be found in Faivre and Schüler (2008), Jogler and Schüler (2009), Komeili (2012), Lower and Bazylinski (2013), and Rahn-Lee and Komeili (2013).

Magnetosome-like structures and magnetic minerals have been demonstrated in eukaryotes, including algae, fish, termites, honey-bees, pigeons, and even in humans, and in some cases they appear to be used for orientation purposes (Kirschvink *et al.*, 2001; Walker *et al.*, 2002). The strict control over the biomineralisation in magnetosomes is reminiscent of that found in the formation of silica shells by diatoms and of tooth and bone formation in animals. Further, magnetosome-like chains of magnetite survive over long periods of geological time in sediments, enabling geobiologists to use bacterial magnetite as 'magnetofossils' to follow the evolution of the history of life in ancient rocks. This led to the hypothesis that magnetosomes may represent one of the most ancient biomineralisation systems, which has been progressively adapted to accommodate the formation of the biominerals found in eukaryotic organisms (Kirschvink and Hagedorn, 2000).
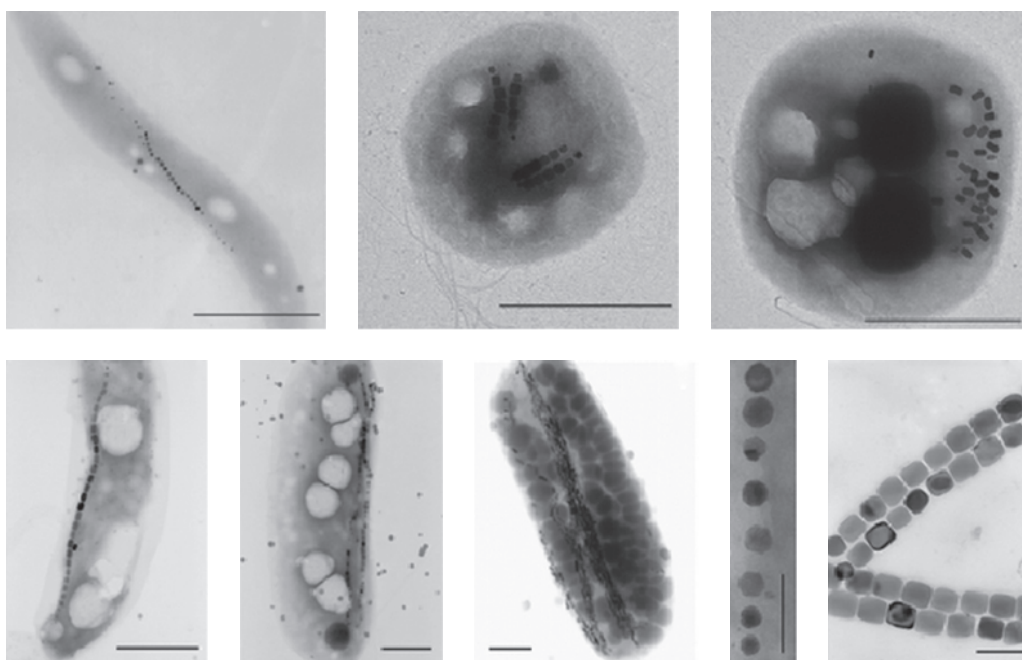

Figure 1.9   *Electron micrographs of various magnetotactic bacteria and magnetosome chains, illustrating the diversity of the cell morphology, of the magnetosome, and of the arrangement of magnetosomes in bacteria. From Faivre, D. and Schüler, D. (2008)*

Comparative genomic analyses have shown that the genes encoding most of the magnetosome-specific proteins, termed *mam* (magnetosome membrane) genes, are organised within a discrete region of the bacterial genome, termed the magnetosome island (MAI), with many of the characteristics of genomic islands often associated with pathogenic organisms (see section on pathogenicity islands in Chapter 4). These genes appear to be involved in the formation of the magnetosome membrane, the biomineralisation of magnetite, and organisation of the magnetosome chain.

The number of MTBs which have been isolated and cultivated in axenic culture has increased considerably during the past few years (for a review, see Lefèvre and Wu, 2013), resulting in a great increase in DNA sequences. Currently, 13 genomic regions which contain the genes responsible for magnetosome production have been sequenced, including the genomes of six cultured MTB and magnetosome gene clusters from seven cultured MTBs (Lefèvre and Wu, 2013). All MTBs have in common a set of genes within the *mamAB* operon (Lefèvre *et al.*, 2013; Richter *et al.*, 2007), which have recently been shown to be crucial for magnetite biomineralisation (Lohsse *et al.*, 2011; Murat *et al.*, 2010; Ullrich and Schüler, 2010). Ten of these genes (*mamABEIKLMOPQ*) are conserved in all magnetite-producing MTB, whereas only nine of them – the exception being *mamL* – seem to be conserved in the two greigite-producing MTB (Lefèvre *et al.*, 2013).

The functions of several of these genes and their associated proteins in magnetosome synthesis and construction of the magnetosome chain have begun to be elucidated through bioinformatics and/or experimental evidence (Komeili, 2012; Lohsse *et al.*, 2011; Murat *et al.*, 2010), and will be discussed below. As proposed by Komeili (2012), in which more details can be found, magnetosome formation has been divided into four stages: (i) biogenesis of the magnetosome membrane; (ii) magnetosome protein sorting; (iii) magnetosome chain formation; and (iv) biomineralisation. A model for magnetosome formation is finally presented.

1.7.1 Biogenesis of the Magnetosome Membrane

It has been clear for some time that the magnetosome membrane originates from the inner cell membrane, and four proteins have been identified from comprehensive genetic analysis to be involved in the formation of the magnetosome membrane (Murat *et al.*, 2010). These are MamI and MamL, which are MTB-specific proteins (Richter *et al.*, 2007) involved in invagination of the magnetosome membrane (Murat *et al.*, 2010), and MamB and MamQ, which are part of large families conserved beyond MTBs. MamB is a member of the cation diffusion facilitator (CDF) family which may be involved in iron transport as well as in magnetosome membrane assembly (Uebe *et al.*, 2011). MamQ has a LemA domain, a ~40-residue helix-loop-helix fold conserved in prokaryotic DNA/RNA-binding proteins (Lin *et al.*, 2000), and also appears to be involved in invagination of the magnetosome membrane (Lohsse *et al.*, 2011; Murat *et al.*, 2010). Other factors are likely to be involved, including possibley MamY (Tanaka *et al.*, 2006).

1.7.2 Protein Sorting

Approximately 20-40 proteins are localised or enriched in the magnetosome membrane (Grünberg *et al.*, 2001, 2004), and the surface of the membrane seems to be covered in a layer of magnetosome proteins (Yamamota *et al.*, 2010), including Mam A, which has a tetratricopeptide repeat (TPR) and is required for vesicle activation (Komeili *et al.*, 2004; Zeytuni *et al.*, 2011; Yamamoto *et al.*, 2010). The X-ray structure of MamA (Zeytuni *et al.*, 2011) sheds light on the way in which it self-assembles and may provide surfaces for binding of other proteins to the magnetosome membrane. Mam E – like MamA and MamP – has a PDZ domain (a common structural domain of 80–90 amino acids found in signalling proteins), which could mediate protein–protein interactions.

This would be compatible with the proposition that it recruits other proteins to the magnetosome membrane (Lohsse *et al*., 2011; Murat *et al*., 2010; Quinlan *et al*., 2011).

1.7.3   Chain Formation

Individual magnetosomes need to be organised into chains in order to orient the cell in a magnetic field. The presence of filaments with dimensions similar to actin filaments alongside the magnetosome chain (Scheffel *et al*., 2006; Komeili *et al*., 2006; Katzmann *et al*., 2010), together with the presence of MamK, an actin-like filamentous protein encoded by one of the genes of the MAI (Grünberg *et al*., 2001), suggested that MamK might provide a structural scaffold for the organisation of the magnetome chain (Scheffel *et al*., 2006; Komeili *et al*., 2006; Taoka *et al*., 2007), probably as the structural component of its cytoskeleton. Like traditional actins, MamK forms dynamic filaments that require an intact NTPase motif for their turnover *in vivo*. Two acidic proteins, MamJ and LimJ, are thought to function as regulators of the dynamic behaviour of MamK filaments (Scheffel *et al*., 2006; Komeili *et al*., 2006; Draper *et al*., 2011).

1.7.4   Biomineralisation

Despite tremendous advances in the present understanding of the genes involved and the possible roles of the proteins encoded by these genes, the current understanding of iron chemistry involved in biomineralisation lags behind. Magnetite formation is achieved by a process of mineralisation which involves: (i) a reductive uptake of iron from the external environment of the bacterial cell, and its transport (perhaps as ferritin) across the magnetosome membrane; (ii) an accumulation of iron within the precursor of the vesicular structure of the magnetosome; (iii) transformation of the initial iron deposit (most likely in the form of ferrihydrite) into magnetite; and (iv) crystallisation of the magnetite mineral to give a particle within the vesicle of a specific size and orientation. The MamP, MamE and MamT proteins have a double MTB-specific *c*-type cytochrome domain that possibly ensures redox control and Fe^{2+}/Fe^{3+} stoichiometry, and may contribute to the process of biocrystallisation (Siponen *et al*., 2012).

The results of initial studies by Frankel *et al*. (1983), using Mössbauer spectroscopy, suggested three different phases in the biomineralisation step: a low-density-hydrous ferric oxide, followed by a high-density-hydrous ferric oxide (namely ferrihydrite [Fh]), which on partial reduction transforms to magnetite. A subsequent Mössbauer study implied a pathway from membrane-bound ferritin, which together with ferrous iron led to the coprecipitation of magnetite (Faivre *et al*., 2007). In a real-time *in vivo* study of *Magnetospirillum gryphiswaldense* magnetosome formation using X-ray magnetic circular dichroism, it was concluded that haematite (α-Fe_2O_3) was a precursor to magnetite (Staniland *et al*., 2007). A more recent study using Fe K-edge X-ray absorption near-edge structure (XANES) and high-resolution transmission electron microscopy (TEM) confirmed ferrihydrite, in the form of bacterial ferritin cores characterised by a poorly crystalline structure and high phosphorus content, as the source of iron for magnetite formation (Fdez-Gubieda *et al*., 2013). Magnetite formation through phase transformation from a highly disordered phosphate-rich ferric hydroxide phase, consistent with prokaryotic ferritins, via transient nanometric ferric (oxyhydr)oxide intermediates within the magnetosome organelle, has been confirmed using X-ray absorption spectroscopy at cryogenic temperatures and TEM imaging techniques (Baumgartner *et al*., 2013a). These results bear a remarkable resemblance to recent findings of synthetic magnetite formation in solution (Baumgartner *et al*., 2013b).

A small subset of magnetosome membrane proteins, encoded by genes of the *mamCD* and *mms6* gene clusters, which are adjacent to one another in the MAI, are tightly associated with the magnetite crystal. These proteins – Mms5, Mms6, Mms7 (MamC), and Mms13 (MamD) – have common

features in their amino acid sequences, including hydrophobic N-terminal and hydrophilic C-terminal regions which contain dense carboxyl and hydroxyl groups that bind iron ions (Arakaki *et al.*, 2003). It has been proposed that Mms6 is involved in the regulation of crystal morphology during magnetite mineralisation (Tanaka *et al.*, 2010), and that the proteins MamGFDC, while not required for magnetite crystallisation, regulate the size of the magnetosome crystals (Scheffel *et al.*, 2008).

1.7.5 A Model for Magnetosome Formation

A possible model for magnetosome formation has been proposed recently (Figure 1.10), which incorporates much of the information described above (Komeili, 2012). In the first step, reshaping
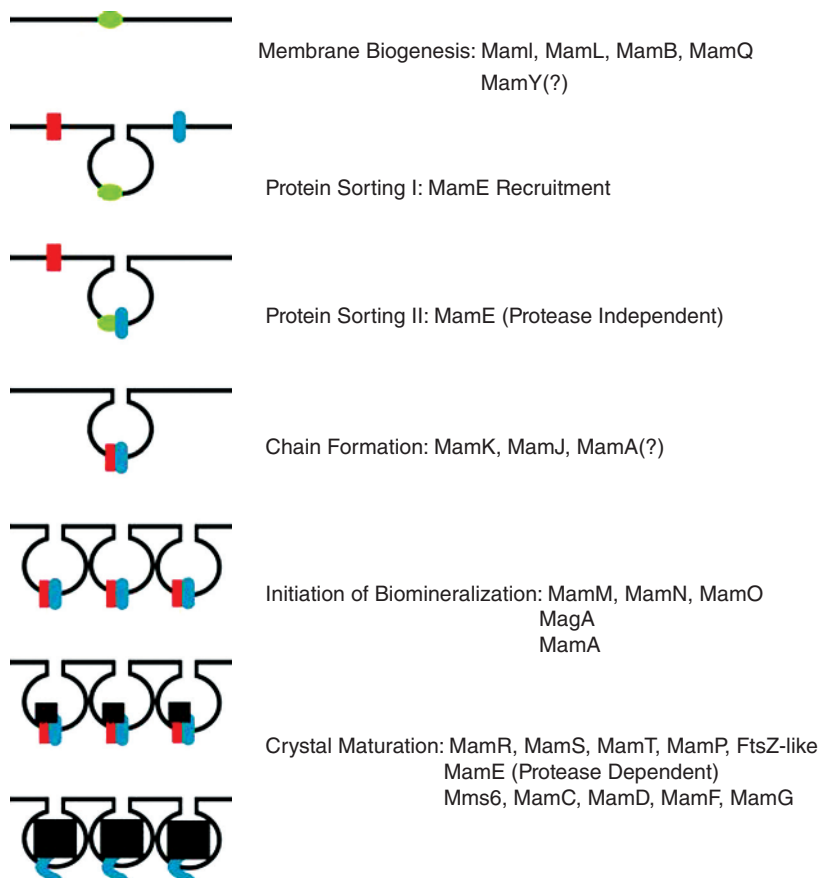

Membrane Biogenesis: MamI, MamL, MamB, MamQ
MamY(?)

Protein Sorting I: MamE Recruitment

Protein Sorting II: MamE (Protease Independent)

Chain Formation: MamK, MamJ, MamA(?)

Initiation of Biomineralization: MamM, MamN, MamO
MagA
MamA

Crystal Maturation: MamR, MamS, MamT, MamP, FtsZ-like
MamE (Protease Dependent)
Mms6, MamC, MamD, MamF, MamG

Figure 1.10 *A model for magnetosome formation. Based on numerous studies, one possible model for magnetosome formation is proposed here. First, the reshaping of the inner cell membrane by MamI, MamL, MamQ, MamB and other factors (green) creates the magnetosome membrane. Second, MamE is recruited to the nascent magnetosome. Third, MamE (in blue), independent of its protease activity, recruits other proteins (red) to the magnetosome. Fourth, MamK and MamJ help to organise magnetosomes into chains. Note that this step is independent of biomineralisation and may occur before or after crystal formation. Fifth, biomineralisation is initiated and small crystals of magnetite are formed. Finally, these small crystals are matured into large crystals in a step that requires the proteolytic activity of MamE. From Komeili (2012)*

of the inner cell membrane by MamI, MamL, MamQ, MamB and other factors creates the magnetosome membrane. In the second step, MamE is recruited to the nascent magnetosome, and in a third step MamE (independent of its protease activity) recruits other proteins to the magnetosome. In step four, MamK and MamJ help to organise magnetosomes into chains (this step is independent of biomineralisation, and may occur before or after crystal formation), while in step five biomineralisation is initiated and small crystals of magnetite are formed. In the final step, these small crystals mature into large crystals in a process that requires not only the proteolytic activity of MamE but also a number of other factors, including the Mms proteins.

References

Arakaki, A., Webb, J. and Matsunaga, T. (2003) A novel protein tightly bound to bacterial magnetic particles in *Magnetospirillum magneticum* strain AMB-1. *J. Biol. Chem.*, **278**, 8745–8750.

Bäuerlein, E. (ed.) (2000) *The Biomineralization of Nano- and Micro-Structures*. Wiley-VCH, Weinheim.

Baumgartner, J., Morin, G., Menguy, N., Perez Gonzalez, T., *et al*. (2013a) Magnetotactic bacteria form magnetite from a phosphate-rich ferric hydroxide via nanometric ferric (oxyhydr)oxide intermediates. *Proc. Natl Acad. Sci. USA*, **110**, 14883–14888.

Baumgartner, J., Dey, A., Bomans, P.H., Le Coadou, C., *et al*. (2013b) Nucleation and growth of magnetite from solution. *Nat. Mater.*, **12**, 310–314.

Berquo, T.S., Banerjee, S.K., Ford, R.G., Penn, R.L. and Pichler, T. (2007) High crystallinity Si-ferrihydrite: an insight into its Neel temperature and size dependence of magnetic properties. *J. Geophys. Res.-Sol. Ea.*, **112**, B02.

Berquo, T.S., Erbs, J.J., Lindquist, A., Penn, R.L. and Banerjee, S.K. (2009) Effects of magnetic interactions in antiferromagnetic ferrihydrite particles. *J. Phys. Condens. Matter*, **21**, 176005.

Billinge, S.J.L. and Kanatzidis, M.G. (2004) Beyond crystallography: the study of disorder, nanocrystallinity and crystallographically challenged materials with pair distribution functions. *Chem. Commun.*, **7**, 749–760.

Bishop, J.L., Pieters, C.M., Burns, R.G., Edwards, J.O., *et al*. (1995) Reflectance spectroscopy of ferric sulfate-bearing montmorillonites as Mars soil analog materials. *Icarus*, **117**, 101–119.

Blakemore, R. (1975) Magnetotactic bacteria. *Science*, **190**, 377–379.

Blakemore, R.P. (1982) Magnetotactic bacteria. *Annu. Rev. Microbiol.*, **36**, 217–238.

Cabello, E., Morales, M.P., Serna, C.J., Barron, V. and Torrent, J. (2009) Magnetic enhancement during the crystallization of ferrihydrite at 25° and 30°C. *Clays Clay Miner.*, **57**, 46–53.

Carta, D., Casula, M.F., Carrias, A., Falqui, A., *et al*. (2009) Structural and magnetic characterization of synthetic ferrihydrite nanoparticles. *Mater. Chem. Phys.*, **113**, 349–355.

Casey, W.H. (2006) Large aqueous aluminium hydroxide molecules. *Chem. Rev.*, **106**, 1–16.

Chukrov, F.V., Zvyagin, B.B., Gorshkov, A.I., Yermilova, L.P. and Balashova, V.V. (1974) Ferrihydrite. *Int. Geol. Rev.*, **16**, 1131–1143.

Coey, J.M.D. and Readman, P.W. (1973) New spin structure in an amorphous ferric gel. *Nature*, **246**, 476–478.

Cornell, R.M., Giovanoli, R. and Schneider, W. (1989) Review of the hydrolysis of iron(III) and the crystallization of amorphous iron(III) hydroxide hydrate. *J. Chem. Tech. Biotech.*, **46**, 115–134.

Crichton, R.R. and Pierre, J.-L. (2001) Old iron, young copper: from Mars to Venus. *Biometals*, **14**, 99–112.

Draper, O., Byrne, M.E., Li, Z., Keyhani, S., *et al*. (2011) MamK, a bacterial actin, forms dynamic filaments in vivo that are regulated by the acidic proteins MamJ and LimJ. *Mol. Microbiol.*, **82**, 342–354.

Drits, V.A., Sakharov, B.A., Salyn, A.L. and Manceau, A. (1993) The structure of six-line ferrihydrite, *Clay Miner.*, **28**, 185.

Faivre, D. and Schüler, D. (2008) Lagnetetactic bacteria and magnetosomes. *Chem. Rev.*, **108**, 4875–4898.

Faivre, D., Böttger, L.H., Matzanke, B.F. and Schüler, D. (2007) Intracellular magnetite biomineralization in bacteria proceeds by a distinct pathway involving membrane-bound ferritin and an iron(II) species. *Angew. Chem. Int. Ed. Engl.*, **46**, 8495–8499.

Fdez-Gubieda, M.L., Muela, A., Alonso, J., García-Prieto, A., *et al*. (2013) Magnetite biomineralization in *Magnetospirillum gryphiswaldense*: time-resolved magnetic and structural studies. *ACS Nano.*, **7**, 3297–3305.

Feng, W. and Nansheng, D. (2000) Photochemistry of hydrolytic iron(III) species and photoinduced degradation of organic compounds. A minireview. *Chemosphere*, **41**, 1137–1147.

Fenton, H.J.H. (1894) The oxidation of tartaric acid in presence of iron. *J. Chem. Soc. Trans.*, **10**, 157–158.

Flynn, C.M., Jr (1984) Hydrolysis of inorganic iron (III) salts. *Chem. Rev.*, **84**, 31–41.

Ford R.G., Bertsch, P.M. and Farley, K.J. (1997) Changes in transition and heavy metal partitioning during hydrous iron oxide ageing. *Environ. Sci. Technol.*, **31**, 2028–2033.

Fortin, D. and Langley, S. (2005) Formation and occurrence of biogenic iron-rich minerals. *Earth Sci. Rev.*, **72**, 1–19.

Frankel, R.B., Papaefthymiou, G.C., Blakemore, R.P. and O'Brien, W. (1983) Fe_3O_4 precipitation in magnetotactic bacteria. *Biochim. Biophys. Acta*, **763**, 147–159.

Géhin, A., Ruby, C., Abdelmoula, M., Benali, O., *et al*. (2002) Synthesis of Fe(II-III) hydroxysulphate green rust by coprecipitation *Solid State Sci.*, **4**, 61–66**.**

Grünberg, K., Wawer, C., Tebo, B.M. and Schüler, D. (2001) A large gene cluster encoding several magnetosome proteins is conserved in different species of magnetotactic bacteria. *Appl. Environ. Microbiol.*, **67**, 4573–4582.

Grünberg, K., Müller, E.C., Otto, A., Reszka, R, *et al*. (2004) Biochemical and proteomic analysis of the magnetosome membrane in *Magnetospirillum gryphiswaldense*. *Appl. Environ. Microbiol.*, **70**, 1040–1050.

Haber, F. and Weiss, J. (1934) The catalytic decomposition of hydrogen peroxide by iron salts. *Proc. Roy. Soc. Ser. A*, **147**, 332–351.

Haber, F. and Willstätter, R. (1931) Unpaarigheit und Radikalketten in Reaktion-Mechanismus organischer und enzymatitischer Vorgänge. *Chem. Ber.*, **64**, 2844–2856.

Halliwell, B. and Gutteridge, J.M.C. (1984) Oxygen toxicity, oxygen radicals, transition metals and disease. *Biochem. J.*, **219**, 1–14.

Hellman, H., Laitinen, R.S., Kaila, L, Jalonen, J., *et al*. (2006) Identification of hydrolysis products of $FeCl_3.6H_2O$ by ESI-MS. *J. Mass Spectrom.* **41**, 1421–1429.

Hiemstra, T. and Van Riemsdijk, W.H. (2009) A surface structural model for ferrihydrite I: Sites related to primary charge, molar mass, and mass density. *Geochim. Cosmochim. Acta*, **73**, 4423–4436.

Hochella, M.F., Jr, Lower, S.K., Maurice, P.A., Penn, R.L., *et al*. (2008) Nanominerals, mineral nanoparticles, and Earth systems. *Science*, **319**, 1631–1635.

Huffman, G.P., Ganguly, B., Zhao, J., Rao, K R.P.M., *et al*. (1993) Structure and dispersion of iron-based catalysts for direct coal liquefaction. *Energy Fuels*, **7**, 285–296.

Jambor, J.L. and Dutrizac, J.E. (1998) Occurrence and constitution of natural and synthetic ferrihydrite, a widespread iron oxyhydroxide. *Chem. Rev.*, **98**, 2549–2585.

Janney, D.E., Cowley, J.M. and Buseck, P.R. (2000) Structure of synthetic 2-line ferrihydrite by electron nanodiffraction. *Am. Miner.*, **85**, 1180–1187.

Janney, D.E., Cowley, J.M. and Buseck, P.R. (2001) Structure of synthetic 6-line ferrihydrite by electron nanodiffraction. *Am. Miner.*, **86**, 327–335.

Jansen, E., Kyek, A., Schafer, W. and Schwertmann, U. (2002) The structure of six-line ferrihydrite, *Appl. Phys. Mater. Sci. Process.*, **74**, S1004–S1006.

Jogler, C. and Schüler, D. (2009) Genomics, genetics, and cell biology of magnetosome formation. *Annu. Rev. Microbiol.*, **63**, 501–521.

Jolivet, J.-P. (2000) *Metal Oxide Chemistry and Synthesis. From Solution to Solid State*. John Wiley & Sons, Chichester.

Jolivet, J.-P., Chanéac, C. and Trone, E. (2004) Iron oxide chemistry. From molecular clusters to extended solid networks. *Chem. Commun*., 481–487.

Jones, L.F., Batsanov, A., Brechin, E.C., Collison, D., *et al*. (2002) Octametallic and hexadecametallic ferric wheels. *Angew. Chem., Int. Ed. Engl*., **41**, 4318–4321.

Katzmann, E, Scheffel, A., Gruska, M., Plitzko, J.M. and Schüler, D. (2010) Loss of the actin-like protein MamK has pleiotropic effects on magnetosome formation and chain assembly in *Magnetospirillum gryphiswaldense*. *Mol. Microbiol.*, **77**, 208–224.

Kirschvink, J.L. and Hagedorn, J.W. (2000) in *The Biomineralization of Nano- and Micro-Structures* (ed. E. Bäuerlein), Wiley-VCH, Weinheim, pp. 1139–1150.

Kirschvink, J.L., Walker, M.M. and Diebel, C.E. (2001) Magnetite-based magnetoreception. *Curr. Opin. Neurobiol.*, **11**, 462–467.

Komeili, A. (2012) Molecular mechanisms of compartmentalization and biomineralization in magnetotactic bacteria. *FEMS Microbiol. Rev.*, **36**, 232–255.

Komeili, A., Vali, H., Beveridge, T.J. and Newman, D.K. (2004) Magnetosome vesicles are present before magnetite formation, and MamA is required for their activation. *Proc. Natl Acad. Sci. USA*, **101**, 3839–3844.

Komeili, A., Li, Z., Newman, D.K. and Jensen, G.J. (2006) Magnetosomes are cell membrane invaginations organized by the actin-like protein MamK. *Science*, **311**, 242–245.

Lefèvre, C.T. and Wu, L.-F. (2013) Evolution of the bacterial organelle responsible for magnetotaxis. *Trends Microbiol.*, **21**, 534–543.

Lefèvre, C.T., Trubitsyn, D., Abreu, F., Kolinko, S., *et al*. (2013) Comparative genomic analysis of magnetotactic bacteria from the Deltaproteobacteria provides new insights into magnetite and greigite magnetosome genes required for magnetotaxis. *Environ. Microbiol.*, **15**, 2712–2735.

Li, Z., Zhang, T. and Li, K. (2011) One-step synthesis of mesoporous two-line ferrihydrite for effective elimination of arsenic contaminants from natural water. *Dalton Trans.*, **40**, 2062–2066.

Lin, F., Blake, D.L., Callebaut, I. and Skerjanc, I.S. (2000). MAN1, an inner nuclear membrane protein that shares the LEM domain with lamina-associated polypeptide 2 and emerin. *J. Biol. Chem.*, **275**, 4840–4847.

Lippard, S.J. (1988) Oxo-bridged polyiron centers in biology and chemistry. *Angew. Chem., Int. Ed. Engl*., **27**, 344–361.

Lohsse, A., Ullrich, S., Katzmann, E., Borg, S., *et al*. (2011) Functional analysis of the magnetosome island in *Magnetospirillum gryphiswaldense*: the mamAB operon is sufficient for magnetite biomineralization. *PLoS ONE*, **6**, e25561.

Lower, B.H. and Bazylinski, D.A. (2013) The bacterial magnetosome: a unique prokaryotic organelle. *J. Mol. Microbiol. Biotechnol.*, **23**, 63–80.

Maillot, F., Morin, G., Wang, Y., Bonnin, D., *et al*. (2011) New insight into the structure of nanocrystalline ferrihydrite: EXAFS evidence for tetrahedrally coordinated iron(III). *Geochim. Cosmochim. Acta*, **75**, 2708–2720.

Manceau, A. (2009) Evaluation of the structural model for ferrihydrite derived from real-space modelling of high-energy X-ray diffraction data. *Clay Miner.*, **44,** 19–34**.**

Mann, S. (1988) Molecular recognition in biomineralization. *Nature*, **332**, 119–124.

Mann, S. (2007) in *Biominerals and Biomineralization* (eds I. Bertini, H.B. Gray, E.I. Stiefel and J.S. Valentine), University Science Books, Sausalito, California, pp. 79–94.

Michel, F.M., Ehm, L., Antao, S.M., Lee, P.L., *et al*. (2007a) The structure of ferrihydrite, a nanocrystalline material. *Science*, **316**, 1726–1729.

Michel, F.M., Ehm, L., Liu, G., Han, W.Q., *et al*. (2007b) Similarities in 2- and 6-line ferrihydrite based on pair distribution function analysis of X-ray total scattering. *Chem. Mater.*, **19**, 1489–1496.

Michel, F.M., Barrón, V., Torrent, J., Morales, M.P., *et al*. (2010) Ordered ferrimagnetic form of ferrihydrite reveals links among structure, composition, and magnetism. *Proc. Natl Acad. Sci. USA*, **107**, 2787–2792.

Murat, D., Quinlan, A., Vali, H. and Komeili, A. (2010) Comprehensive genetic dissection of the magnetosome gene island reveals the step-wise assembly of a prokaryotic organelle. *Proc. Natl Acad. Sci. USA*, **107**, 5593–5598.

Nudelman, F. and Sommerdijk, N.A. (2012) Biomineralization as an inspiration for materials chemistry. *Angew. Chem.*, **51**, 6582–6596.

Pannalai, S.J., Crowe, S.A., Cioppa, M.T., Symons, D.T.A., *et al*. (2005) Room-temperature magnetic properties of ferrihydrite: A potential magnetic remanence carrier? *Earth Planet Sci*. *Lett.*, **236**, 856–870.

Pankhurst, Q.A. and Pollard, R.J. (1992) Structural and magnetic properties of ferrihydrite. *Clays Clay Miner.*, **40**, 268–272.

Pearson, R.G. (1963) Hard and soft acids and bases. *J. Am. Chem. Soc.*, **85**, 3533–3539.

Pierre, J.-L. and Fontecave, M. (1999) Iron and activated oxygen species in biology: the basic chemistry. *Biometals*, **12**, 195–199.

Quinlan, A., Murat, D., Vali, H. and Komeili, A. (2011) The HtrA/DegP family protease MamE is a bifunctional protein with roles in magnetosome protein localization and magnetite biomineralization. *Mol. Microbiol.*, **80**, 1075–1087.

Rahn-Lee, L. and Komeili, A. (2013) The magnetosome model: insights into the mechanisms of bacterial biomineralization. *Front. Microbiol.*, **4**, Article 352.

Rancourt, D.G. and Meunier, J.F. (2008) Constraints on structural models of ferrihydrite as a nanocrystalline material. *Am. Miner.*, **93**, 1412–1417.

Rancourt, D.G., Fortin, D., Pichler, T., Thibault, P.-J., *et al*. (2001) Mineralogy of a natural As-rich hydrous ferric oxide coprecipitate formed by mixing of hydrothermal fluid and seawater: Implications regarding surface complexation and color banding in ferrihydrite deposits. *Am. Miner.*, **86**, 834–851.

Refait, P.H., Abdelmoula, M. and Géhin, J.-M.R. (1998) Mechanisms of formation and structure of green rust one in aqueous corrosion of iron in the presence of chloride ions. *Corros. Sci.*, **40**, 1547–1560.

Richter, M., Kube, M., Bazylinski, D.A., Lombardot, T., *et al*. (2007) Comparative genome analysis of four magnetotactic bacteria reveals a complex set of group-specific genes implicated in magnetosome biomineralization and function. *J. Bacteriol.*, **13**. 4899–4910.

Riveros, P.A., Dutrizac, J.E. and Spencer, P. (2001) Arsenic disposal practices in the metallurgical industry. *Can. Metall. Q.*, **40**, 395–420.

Scheffel, A., Gruska, M., Faivre, D., Linaroudis, A., *et al*. (2006) An acidic protein aligns magnetosomes along a filamentous structure in magnetotactic bacteria. *Nature*, **440**, 110–114.

Scheffel, A., Gärdes, A., Grünberg, K., Wanner, G. and Schüler D. (2008) The major magnetosome proteins MamGFDC are not essential for magnetite biomineralization in *Magnetospirillum gryphiswaldense* but regulate the size of magnetosome crystals. *J. Bacteriol.*, **190**, 377–386.

Schmitt, W., Murugesu, M., Goodwin, J.C., Hill, J.P., *et al*. (2001) Strategies for producing cluster-based magnetic arrays. *Polyhedron*, **20**, 1687–1697.

Schwertmann, U., Carlson, L. and Murad, E. (1987) Properties of iron oxides in two Finnish lakes in relation to the environment of their formation. *Clays Clay Miner.*, **35**, 297–304.

Schwertmann, U., Friedl, J. and Stanjek, H. (1999) From Fe(III) ions to ferrihydrite and then to hematite. *J. Colloid Interface Sci.*, **209**, 215–223.

Siponen, M.I., Adryanczyk, G., Ginet, N., Arnoux, P. and Pignol, D. (2012) Magnetochrome: a c-type cytochrome domain specific to magnetotactic bacteria. *Biochem. Soc. Trans.*, **40**, 1319–1323.

Smith, S.J., Page, K., Kim, H., Campbell, B.J., *et al*. (2012) Novel synthesis and structural analysis of ferrihydrite. *Inorg. Chem.*, **51**, 6421–6424.

Staniland, S., Ward, B., Harrison, A., van der Laan, G. and Telling, N. (2007) Rapid magnetosome formation shown by real-time X-ray magnetic circular dichroism. *Proc. Natl Acad. Sci. USA*, **104**, 19524–19528.

Taft, K.L. and Lippard, S.J. (1990) Synthesis and structure of $[Fe(OMe)_2(O_2CCH_2Cl)]_{10}$: a molecular ferric wheel. *J. Am. Chem. Soc.*, **112**, 9629–9630.

Taft, K.L., Papaefthymiou, G.C. and Lippard, S.J. (1993) A mixed-valent polyiron oxo complex that models the biomineralization of the ferritin core. *Science*, **259**, 1302–1305.

Tanaka, M., Okamura, Y., Arakali, A., Tanaka, T., *et al*. (2006) Origin of magnetosome membrane: proteomic analysis of magnetosome membrane and comparison with cytoplasmic membrane. *Proteomics*, **6**, 5234–5247.

Tanaka, M., Mazuyama, E., Arakaki, A. and Matsunaga, T. (2010) MMS6 protein regulates crystal morphology during nano-sized magnetite biomineralization in vivo. *J. Biol. Chem.*, **286**, 6386–6392.

Taoka, A., Asada, R., Wu, L.F. and Fukumori, Y. (2007) Polymerization of the actin-like protein MamK, which is associated with magnetosomes. *J. Bacteriol.*, **189**, 8737–8740.

Thompson, D.W. (1917) *On growth and form*. Cambridge University Press, Cambridge, pp. 793.

Towe, K.M. (1981) Structural distinction between ferritin and iron-dextran (imferon). An electron diffraction comparison. *J. Biol. Chem*., **256**, 9377–9378.

Towe, K.M. and Bradley, W.F. (1967) Mineralogical constitution of colloidal 'hydrous ferric oxides'. *J. Colloid Interface Sci.*, **24**, 384–392.

Uebe, R., Henn, V. and Schüler, D. (2011) The MagA protein of *Magnetospirilla* is not involved in bacterial magnetite biomineralization. *J. Bacteriol.*, **194**, 1018–1023.

Ullrich, S. and Schüler, D. (2010) Cre-lox-based method for generation of large deletions within the genomic magnetosome island of *Magnetospirillum gryphiswaldense*. *Appl. Environ. Microbiol.*, **76**, 2439–2444.

Walker, M.M., Dennis, T.E. and Kirschvink, J.L. (2002) The magnetic sense and its use in long-distance navigation by animals. *Curr. Opin. Neurobiol.*, **12**, 735–744.

Wilt, F.H. (2005) Developmental biology meets materials science: Morphogenesis of biomineralized structures. *Dev. Biol.*, **280**, 15–25.

Wu, J. and Luther, G.W., III (1996) Spatial and temporal distribution of iron in the surface water of the northwestern Atlantic Ocean. *Geochim. Cosmochim. Acta*, **60**, 2729–2741.

Yamamoto, D., Taoka, A., Uchihashi, T., Sasaki, H., *et al*. (2010) Visualization and structural analysis of the bacterial magnetic organelle magnetosome using atomic force microscopy. *Proc. Natl Acad. Sci. USA*, **107**, 9382–9387.

Zeytuni, N., Ozyamak, E., Ben-Harush, K., Davidov, G., *et al*. (2011) Self-recognition mechanism of MamA, a magnetosome-associated TPR-containing protein, promotes complex assembly. *Proc. Natl Acad. Sci. USA*, **108**, E480–E487.